Occluded Boundary Detection for Small-Footprint Groundborne LIDAR Point Cloud Guided by Last Echo

Zhipeng Cai (蔡志鹏), Cheng Wang (王程), *Member, IEEE*,
Chenglu Wen (温程璐), *Member, IEEE*, and Jonathan Li, *Senior Member, IEEE*

***Abstract*—Occluded boundary detection in a 3-D point cloud is an indispensable preprocessing step for many applications, such as point cloud completion. Meanwhile, existing methods do not have the ability of distinguishing occluded and complete surface borders, such as the border of a sign board. To solve this problem, this letter presents an occluded boundary detection method for small-footprint LIDAR point clouds. The main novelty of this letter is using the last-echo information for occluded boundary detection. Seed boundary (SB) points are subsequently detected using this last-echo information. Finally, the SB points are grown into neighboring points using an occluded boundary growth algorithm. To the best of our knowledge, this method is the first method that uses the last-echo information to detect occluded boundaries. Experimental results with comparisons indicate that the proposed method can accurately and efficiently detect an occluded boundary without contamination from a complete surface border. These advantages allow the proposed method to benefit further applications such as point cloud completion, as demonstrated in the application section.**

***Index Terms*—Last echo, LIDAR, occluded boundary detection, point cloud.**

I. Introduction

THE development of 3-D laser scanners provides convenient means to acquire real-world 3-D point cloud data. Occlusion is a general and inevitable problem that generates shadowlike missing regions in a point cloud during its acquisition. The further processing of point clouds such as object detection [3] and 3-D reconstruction [2] is often affected by occlusion. Occlusion manipulations heavily depend on accurately detecting an occluded boundary. A major difficulty for occluded boundary detection is distinguishing the complete surface border from an occluded boundary. This letter aims to detect the occluded boundary points in a small-footprint groundborne LIDAR point cloud.

In previous literature [4]–[8], researchers considered occlusion detection for 2-D images. Nevertheless, 3-D point clouds differ and are more complex than 2-D images. Some literature focusing on similar topics has been recently published. Bendels [1] proposed a multiclue-filtering-based hole detection method for 3-D point clouds. Wang *et al.* [9] proposed an edge extraction method that merged 3-D point clouds and 2-D images. However, none considered distinguishing an occluded boundary from a complete surface border.

In an airborne laser scanning point cloud, large-footprint multiecho information has been already used in applications such as vegetation filtering [10] and building extraction [11], [12]. However, due to the significant difference in the footprint size between airborne and close-range groundborne LIDAR systems, the characteristics of the last-echo information are significantly different; therefore, the processing method and the potential applications are also quite different.

In most airborne LIDAR systems, the footprint size of a scanner is large. Large-footprint airborne systems have a 10–70-m footprint diameter, and small-footprint airborne systems have a 0.2–3-m footprint diameter, depending on the flying height and the beam divergence. Most of the previous applications are based on large-footprint systems. Small-footprint systems have considerable potential but do not have dedicated applications [13]. With such a large footprint, the last-echo point of airborne LIDAR systems is not suitable for detecting an accurate occluded boundary.

In small-footprint groundborne LIDAR systems, the footprint size is much smaller due to the short distance from the scanner to the target. For instance, for RIEGL VZ-1000 and RIEGL VMX-450, the 100-m footprint diameter is 0.03 m [14].

Small-footprint multiecho LIDAR systems provide the accurate location of an entire backscattered signal for each emitted laser pulse. This multiecho information from the backscattered signal reflects the order for all targets scanned by the same laser pulse. The last echo is the last detected echo from a reflected waveform of a laser pulse; in addition, only the reflection with multiple echoes is concerned, and single-echo reflection does not have a last echo (as shown in Fig. 1). In this letter, we

Manuscript received June 30, 2015; revised August 2, 2015; accepted August 2, 2015. This work was supported by the National Science Foundation of China under Project 61371144.

Z. Cai and C. Wang are with the Fujian Key Laboratory of Sensing and Computing for Smart City, Department of Computer Science, School of Information Science and Engineering, Xiamen University, Xiamen 361005, China (e-mail: czptc2h@gmail.com; cwang@xmu.edu.cn).

C. Wen is with the Fujian Key Laboratory of Sensing and Computing for Smart City, Department of Cognitive Science and Technology, School of Information Science and Engineering, Xiamen University, Xiamen 361005, China (e-mail: clwen@xmu.edu.cn).

J. Li is with the Key Laboratory of Underwater Acoustic Communication and Marine Information Technology (Ministry of Education), Department of Communication Engineering, School of Information Science and Engineering, Xiamen University, Xiamen 361005, China, and also with the GeoSpatial Technology and Remote Sensing Laboratory, Department of Geography and Environmental Management, Faculty of Environment, University of Waterloo, Waterloo, ON N2L 3G1, Canada (e-mail: Junli@xmu.edu.cn).

Color versions of one or more of the figures in this paper are available online at http://ieeexplore.ieee.org.

Digital Object Identifier 10.1109/LGRS.2015.2466811

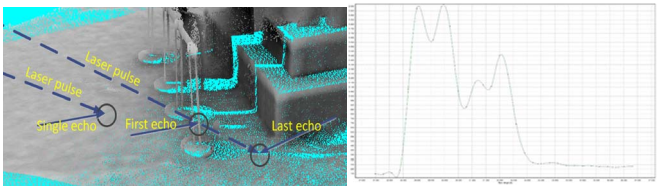

(a) (b)

Fig. 1. Demonstration of full-waveform data and multiecho information.

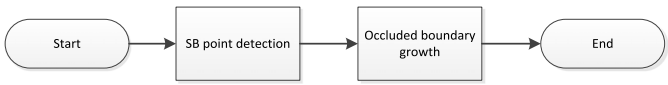

Fig. 2. Workflow for the proposed method.

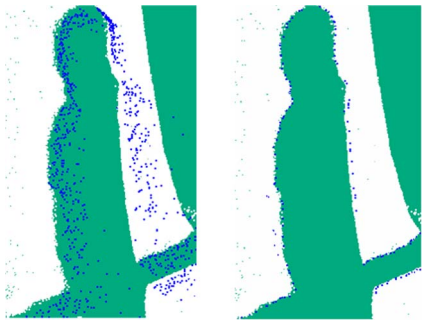

(a) (b)

Fig. 3. Outlier removal. (a) Occluded region with outliers. (b) Occluded region after the outlier removal process. The blue points are the SB points.

propose an original way to make use of the close relationship between the last-echo information and occlusion. Indeed, the last echo allows revealing the location of an occluded boundary. This observation inspired us to generate the proposed method for detecting occluded boundaries.

The proposed method makes three main contributions. First, to the best of our knowledge, we are the first to discover that small-footprint last-echo points are able to help indicate the location of an occluded boundary. Using this property, the occluded boundary is quickly detected, even for large-scale real-world data. In addition, a complete surface border can be distinguished from the occluded boundary using the last-echo information. Second, the outliers near occluded regions are quickly and precisely removed using the indication of the last-echo information. Finally, an occluded boundary growth algorithm increases the detection rate for occluded boundary points.

II. Methodology

The workflow for the proposed method is shown in Fig. 2. All seed boundary (SB) points are first extracted using the last-echo information to indicate the occluded region. With the problem of the low density of SB points, an occluded boundary growth algorithm is then proposed to extract all the occluded boundary points.

A. SB Point Detection

There are many small-footprint LIDAR systems capable of acquiring the last-echo information. However, the potential of this information has not yet been realized. The major problem with detecting an occluded boundary is distinguishing occluded boundary points from complete surface boundary points. Building a mathematical model for occlusion is difficult in a 3-D space. Therefore, we proposed a novel usage of the last-echo information in small-footprint groundborne LIDAR systems to precisely detect an occluded boundary.

In a small-footprint multiecho LIDAR system, a scanner emits a laser pulse to scan an object and records all the backscattered signals of the same laser pulse. As shown in Fig. 1(a), multiple echoes are generated when a laser pulse is incompletely blocked by the front object and illuminates the objects behind it. As shown in Fig. 1(b), the order for each echo is recorded according to the time the laser pulse hits the corresponding object. Therefore, multiecho information reveals the order of the different objects scanned by the same laser pulse. Of the generated multiple echo points, the last-echo points are the last hit by the laser pulse, and they are occluded by the front objects. Thus, the last-echo points indicate the location of occluded boundaries.

The last-echo information is provided by commercial LIDAR systems, such as the RIEGL VZ-1000 and VMX-450 systems. We label all of the extracted last-echo points as SB points. Using this indication, the proposed method avoids detecting the complete surface border that is not generated by the occlusion.

Due to the occlusion, the acquired coordinate accuracy for the last-echo points is not trustworthy. A LIDAR system uses the time-of-flight principle to compute the distance between the laser scanner and the target as follows:

$$S = \frac{cn}{2f} \tag{1}$$

where S is the distance to the target, c is the speed of light, n is the number of returned signals received by the sensor, and f is the frequency of the oscillator. When occlusion occurs, only part of the laser beam illuminates the target. Thus, some of the returned signals for the last-echo point may have a lower intensity than the signal detection threshold, which lowers the measured n in (1) from the real number. Consequently, the measured distance to the target may be lower than the real distance, which produces erroneous last-echo points. Therefore, the initially detected SB points usually include outliers [as shown in Fig. 3(a)]. Additionally, when the returned signal disappears, no last-echo point will be detected. As a result, the density of the SB points is usually low.

This phenomenon affects the performance of many applications, such as point cloud completion and reconstruction. Based on these observations, we propose an efficient two-step outlier removal process with the following steps: 1) remove all last-echo points; and 2) find for each removed last-echo point a nearest point to be the new SB point. Fig. 3(a) shows an occluded region filled with outliers. All of the blue points were the first detected SB points. Fig. 3(b) shows the same region after removing all the last-echo points and after detecting new SB points (painted in blue). In this way, most of the outliers were removed, and the occluded boundary contour was accurately detected.

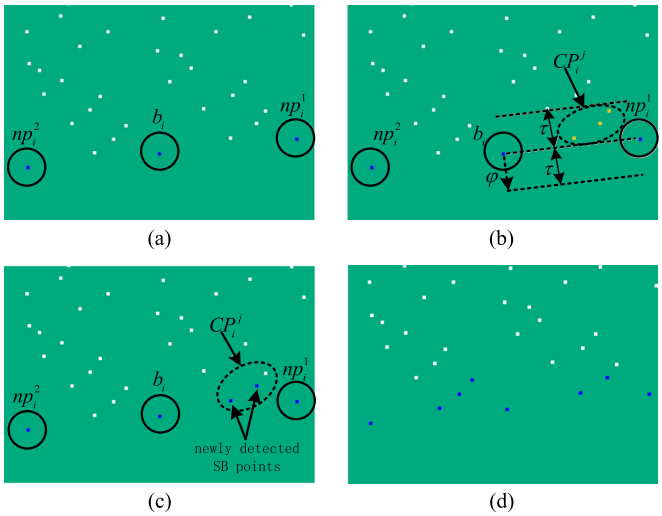

Fig. 4. Occluded boundary growth algorithm. (a) Result of the SB point detection. (b) Extracting CP_i^1 between b_i and np_i^1. (c) Newly detected SB points between b_i and np_i^1. (d) Result of the occluded boundary growth.

B. Occluded Boundary Growth Algorithm

The last-echo point density is usually low, which makes it difficult to precisely indicate the entire occluded boundary. Therefore, we propose an occluded boundary growth algorithm to enhance the detected boundary point density and to benefit further applications.

The occluded boundary growth algorithm finds the undetected boundary points near each SB point. The occluded boundary growth algorithm for each SB point consists of three steps (as shown in Fig. 4).

1) For every SB point, i.e., b_i, find np_i^1 and np_i^2, which are the two SB points nearest to and on the opposite sides of b_i. If there are fewer than two points on the opposite sides of b_i within a certain radius, i.e., r, then find as many points as possible. r is defined as follows when P denotes the original point cloud:

$$r = 5 * \min_{p_i, p_j \in P} \|p_i - p_j\| (p_i \neq p_j). \tag{2}$$

Specifically, factor "5" in (2) was set according to our experience. It works well in our data acquired by the RIEGL VZ-1000 and VMX-450 systems. The factor can be turned larger for other LIDAR systems to guarantee the ability of finding np_i^1 and np_i^2. Moreover, the time cost is not heavily affected by the adjustment of parameter r. The efficiency of the proposed method using a different parameter r is shown in Section III-A. np_i^1 is defined as

$$np_i^1 = \begin{cases} \arg\min_{b_j \neq b_i} (\|b_i - b_j\|), & \left(\min_{b_j \neq b_i} (\|b_i - b_j\|) \leq r\right) \\ \varnothing, & \left(\min_{b_j \neq b_i} (\|b_i - b_j\|) > r\right). \end{cases} \tag{3}$$

Let N_{bi} denote the neighbor point set for b_i within a radius r. Define

$$\varphi = \frac{\sum_{p_j \in N_{bi}} (b_i - p_j)}{\left\| \sum_{p_j \in N_{bi}} (b_i - p_j) \right\|} \tag{4}$$

which is the normalized mean vector from all the points of N_{bi} to b_i. np_i^2 is found if $\exists b_k \neq b_i$, such that

$$(v_2 - v_2 \cdot \varphi \cdot \varphi) \cdot (v_1 - v_1 \cdot \varphi \cdot \varphi) < 0 \tag{5}$$

where $v_1 = np_i^1 - b_i$, and $v_2 = b_k - b_i$. Let B_2 denote all the SB points that meet (4); then, np_i^2 is defined as

$$np_i^2 = \begin{cases} \arg\min_{b_k \in B_2} (\|b_k - b_i\|), & \left(\min_{b_k \in B_2} (\|b_i - b_k\|) \leq r\right) \\ \varnothing, & \left(\min_{b_k \in B_2} (\|b_i - b_k\|) > r\right). \end{cases} \tag{6}$$

2) For np_i^j, construct boundary extension line segment l_i^j, and if $\|l_i^j\| > (r/2)$, extract all the points within a distance, i.e., τ, from l_i^j, where

$$\tau = \frac{\sum_{p_j \in N_{bi}} \min_{p_k \neq p_j, p_k \in N_{bi}} \|p_j - p_k\|}{|N_{bi}|}. \tag{7}$$

Using τ as a bounding radius reduces the time cost for the next step. The extracted points are defined by point set CP_i^j.

3) Detect all the boundary points within CP_i^j using the feature proposed by Bendels [1]. The feature for boundary detection contains three parts, i.e., the angle criterion, the half-disk criterion, and the shape criterion, respectively.

The effect of the occluded boundary growth algorithm is demonstrated in the following section.

III. Experimental Results

The experimental test for the proposed method used real-world point cloud data acquired by a RIEGLVZ-1000 system and a RIEGL VMX-450[1] system. Other kinds of laser scanning systems are also able to provide the last-echo information, such as all other RIEGL VZ-Series systems. The proposed method was implemented using C++ and executed on a computer with an Intel Core i3-2120 3.30-GHz central processing unit with 4.0-GB random access memory.

A. Results and Discussion

The result for the proposed method is shown in Fig. 5. The occluded boundary points were precisely detected under various occlusion situations. Because the last echo will not be generated on the complete surface border, complete surface border points [such as the boundary points of the window in Fig. 5(a) and the window of a car in Fig. 5(f)] are perfectly excluded. The density of the boundary points is sufficiently high to provide information for further applications.

The time cost of the proposed method is shown in Table I. For all demonstrated large-scale real-world point clouds, the proposed method was fast.

The efficiency of the proposed method is not heavily related to parameter r. Fig. 6 shows the effect parameter r had on the time cost for four point cloud data. The time cost remained nearly unchanged after increasing r.

[1]Our laser scanning system can be found at http://www.riegl.com/.

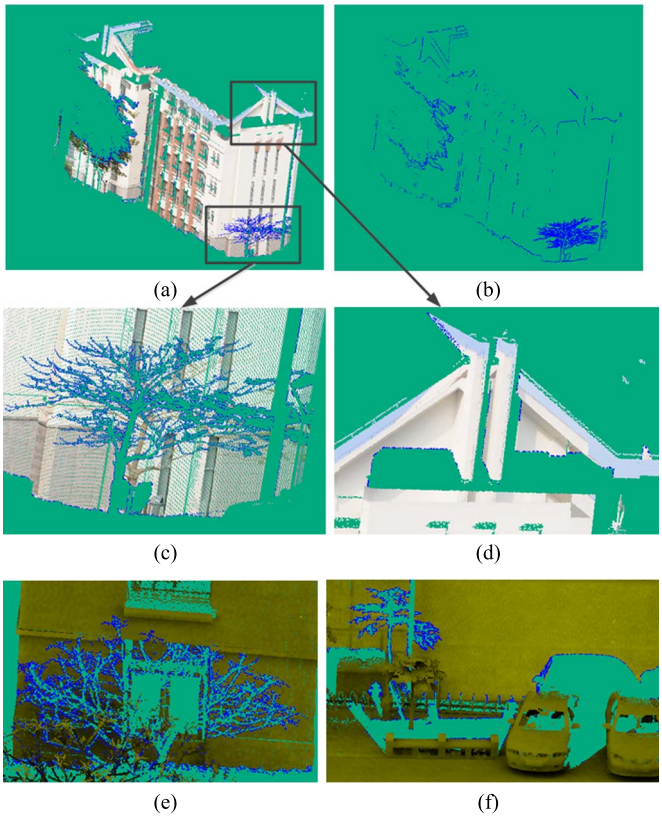

Fig. 5. Results from the proposed method. (a) Detection result of the entire data. (b) Detected occluded boundary points. (c) and (d) Partially enlarged detail of (a). (e) and (f) Other data with different occlusion situations. The blue points are the detected occluded boundary points.

TABLE I
TIME COST OF THE PROPOSED METHOD AND THE METHOD OF BENDELS

Data	number of points	time cost of Bendels and Gerhard [1] (s)	time cost of the proposed method (s)	Time reduction rate
Data 1	815374	30.830	0.360	98.83%
Data 2	6175412	3503.900	1.407	99.96%
Data 3	12031293	11417.700	2.521	99.98%

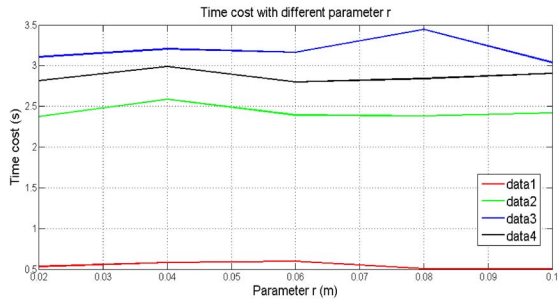

Fig. 6. Time cost for the proposed method with a different parameter r.

The effect of the occluded boundary growth algorithm is shown in Fig. 7. Before the execution of the algorithm, there remain undetected occluded boundary points between each pair of SB points [as shown in Fig. 7(a)]. In contrast, after the occluded boundary growth, most of the undetected occluded boundary points between two SB points are detected [as shown in Fig. 7(b)].

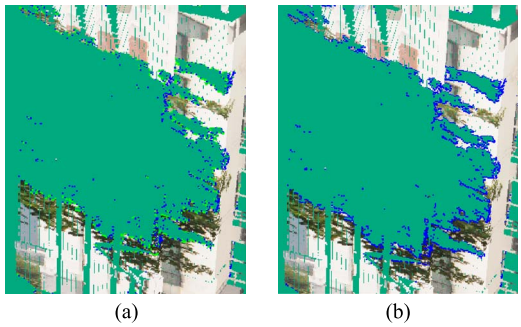

Fig. 7. Result of the occluded boundary growth algorithm. (a) Result before the execution of the algorithm. (b) Result after the execution of the algorithm. The blue points are the detected occluded boundary points.

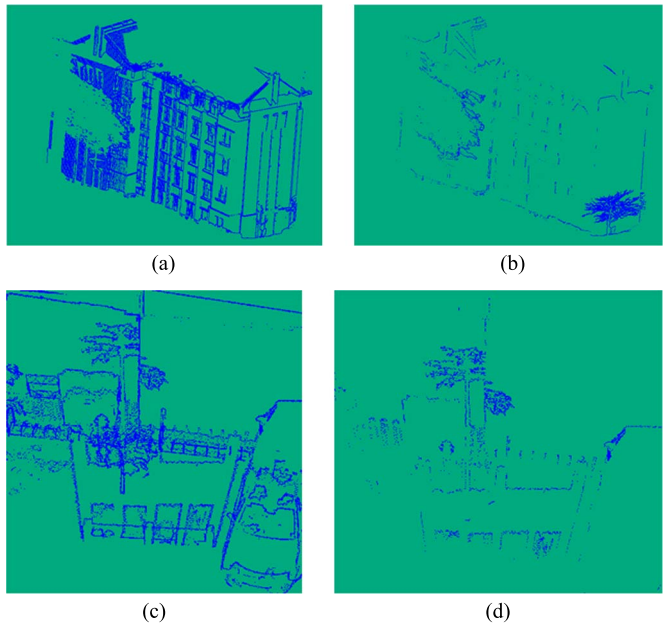

Fig. 8. Comparative results. (Left) Result for the method of Bendels. (Right) Result using the proposed method.

B. Comparison

In this section, we compare the performance of the proposed method with the method of Bendels [1]. As shown in Fig. 8, within two large-scale real-world data, the method of Bendels cannot distinguish the occluded boundary from the complete surface border. The boundary of window frames and the edge of walls that are all complete surface borders are not excluded in Fig. 8(a) and (c). In contrast, the proposed method can not only precisely detect the occluded boundary points but also perfectly exclude the complete surface border.

The time cost and accuracy of the two methods are shown in Tables I and II, respectively. In Table II, Tpr refers to the true-positive rate, and Fpr refers to the false-positive rate. The proposed method utilizes the last-echo information to quickly locate the occluded region. Therefore, the proposed method significantly reduces the time cost for calculating the complex geometric feature throughout all points of the data. When the number of points exceeded 12 million, the method of Bendels cost more than 3 h. In contrast, the proposed method only costs 2.521 s, which is about 500 times faster than the method of Bendels.

TABLE II
ACCURACY MEASUREMENTS OF THE DETECTION RESULT

Result of the proposed method	Tpr of our method	Fpr of our method	Tpr by [1]	Fpr by [1]
Data 4	99.21%	0	26.33%	5.34%
Data 5	96.85%	0	1	28.63%
Data 6	98.15%	0	1	6.13%

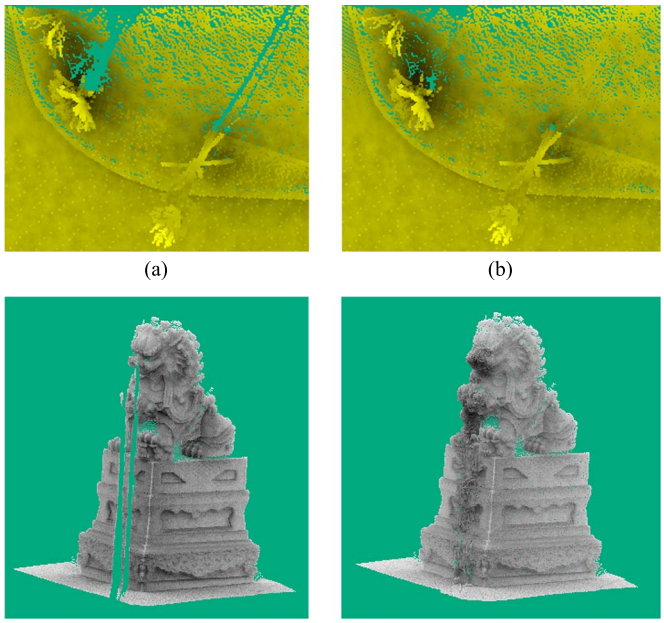

Fig. 9. Application of point cloud completion. (Left) Original data with occlusion. (Right) Completion results using the proposed method.

For accuracy measurements, we manually selected all occluded boundary points to define the ground truth because no standard database for occluded boundary detection in a point cloud exists. In addition, in the experiment, a ground-truth point is considered correctly detected if there is at least one detected occluded boundary point within a certain distance (0.03 m in practice) of the ground-truth point. The proposed method yielded a true-positive rate above 96% with no false-positive points because the last-echo information provides the capability to only extract the occluded boundary points. In contrast, the method of Bendels was sensitive to the density of the neighbor points, and it was unstable for data with different density levels. In Data 4, which are the data in Fig. 5(a), many thin gaps on the wall occluded by the tree branches were not detected by the method of Bendels, which caused a low true-positive rate. For all of the data, the false-positive rate of the method of Bendels was higher than 5% (28.63% for Data 5), which is intolerable because all the data have more than 50 000 points. Thus, there were always over 2500 false detected points, which will lead to unacceptable errors in further applications.

C. Further Study on Point Cloud Completion

The proposed method is able to benefit further applications. Here, we implemented the point cloud completion application that is shown in Fig. 9. We first used the proposed method to accurately detect occluded boundaries, and then, we completed the occluded regions based on the occluded boundaries. In Fig. 9(b) and (d), all of the incomplete regions were perfectly completed.

IV. CONCLUSION

This letter has presented a novel last-echo-based occluded boundary detection method for small-footprint groundborne LIDAR point clouds. First, the innovative use of guidance from the last-echo information allowed the location of an occluded boundary to be quickly and precisely detected through an SB point detection procedure. Outliers near the occluded boundary were precisely removed via an efficient outlier removal process during the SB point detection. Complete surface borders were excluded from the occluded boundary using the last-echo information. An occluded boundary growth algorithm then increased the detection rate of the occluded boundary points. The results from the discussion and comparison reveal the advantages of the proposed method, i.e., high accuracy, a low time cost, and the ability to distinguish an occluded boundary from a complete surface border. Occlusion in structures such as tree leaves is not particularly removed, which may be a limitation for further applications.

REFERENCES

[1] G. H. Bendels, "Detecting holes in point set surfaces," in *Proc. 14th Int. Conf. Central Europe Comput. Graph., Vis. Comput. Vis.*, 2006, pp. 1–8.
[2] A.-L. Chauve, P. Labatut, and J.-P. Pons, "Robust piecewise-planar 3D reconstruction and completion from large-scale unstructured point data," in *Proc. IEEE CVPR*, 2010, pp. 1261–1268.
[3] H. Wang *et al.*, "Object detection in terrestrial laser scanning point clouds based on Hough forest," *IEEE Geosci. Remote Sens. Lett.*, vol. 11, no. 10, pp. 388–396, Oct. 2014.
[4] Y. Xu, L. Qin, G. Li, and Q. Huang, "An efficient occlusion detection method to improve object trackers," in *Proc. IEEE ICIP*, 2013, pp. 2445–2449.
[5] A. Ayvaci, M. Raptis, and S. Soatto, "Occlusion detection and motion estimation with convex optimization," in *Proc. Adv. Neural Inf. Process. Syst.*, 2010, pp. 100–108.
[6] D. Sun, C. Liu, and H. Pfister, "Local layering for joint motion estimation and occlusion detection," in *Proc. IEEE CVPR*, 2014, pp. 1098–1105.
[7] A. N. Stein and M. Hebert, "Occlusion boundaries from motion: Low-level detection and mid-level reasoning," *Int. J. Comput. Vis.*, vol. 82, no. 3, pp. 325–357, May 2009.
[8] P. Sundberg, T. Brox, M. Maire, P. Arbeláez, and J. Malik, "Occlusion boundary detection and figure/ground assignment from optical flow," in *Proc. IEEE CVPR*, 2011, pp. 2233–2240.
[9] Y. Wang, D. Ewert, D. Schilberg, and S. Jeschke, "Edge extraction by merging 3D point cloud and 2D image data," in *Proc. 10th CEWIT*, 2013, pp. 1–6.
[10] G. Vosselman and H.-G. Maas, "Adjustment and filtering of raw laser altimetry data," in *Proc. OEEPE Workshop Airborne Laser Scanning Interferometric SAR Detailed Digital Terrain Models*, Stockholm, Sweden, 2001, pp. 1–11.
[11] G. Zhou and X. Zhou, "Seamless fusion of LiDAR and aerial imagery for building extraction," *IEEE Trans. Geosci. Remote Sci.*, vol. 52, no. 11, pp. 7393–7407, Nov. 2014.
[12] G. Zhou, C. Song, J. Simmers, and P. Cheng, "Urban 3D GIS from LiDAR and digital aerial images," *Comput. Geosci.*, vol. 30, no. 4, pp. 345–353, May 2004.
[13] C. Mallet and F. Bretar, "Full-waveform topographic LIDAR: State-of-the-art," *ISPRS J. Photogramm. Remote Sens.*, vol. 64, no. 1, pp. 1–16, Jan. 2009.
[14] J. L. Carrivick, M. W. Smith, and D. M. Carrivick, "Terrestrial laser scanning to deliver high-resolution topography of the upper Tarfala valley, arctic Sweden," *GFF*, to be published.